Science of the Total Environment 772 (2021) 145044

Contents lists available at ScienceDirect

Science of the Total Environment

journal homepage: www.elsevier.com/locate/scitotenv

HERisk: An improved spatio-temporal human health risks assessment software

Jordan Brizi Neris [a,*], Diango M. Montalván Olivares [b], Caroline Santos Santana [b], PraiseGod Chidozie Emenike [c,d], Fermin G. Velasco [b], Sergio Fred Ribeiro Andrade [b], Caio Marcio Paranhos [a]

[a] Department of Chemistry, Federal University of São Carlos, highway Washington Luis Km 235, CEP 13565-905 São Carlos, São Paulo, Brazil
[b] Department of Exact and Technological Sciences, State University of Santa Cruz, highway Jorge Amado - Km 16, CEP 45662-900 Ilhéus, Bahia, Brazil
[c] Department of Civil Engineering, Covenant University, Ota, Ogun State, Nigeria
[d] Cranfield Water Science Institute, School of Water, Energy and Environment, Cranfield University, MK43 0AL Bedford, United Kingdom

HIGHLIGHTS

- The features of the new HERisk software are in-depth described.
- The usefulness of the code was showcased by assessing the risks in a mining area.
- Contents of potentially toxic elements in soils and surface waters were studied.
- Mining and agricultural activities are responsible for the pollution of the region.
- The entire area around the mine presents a high risk for human health.

GRAPHICAL ABSTRACT

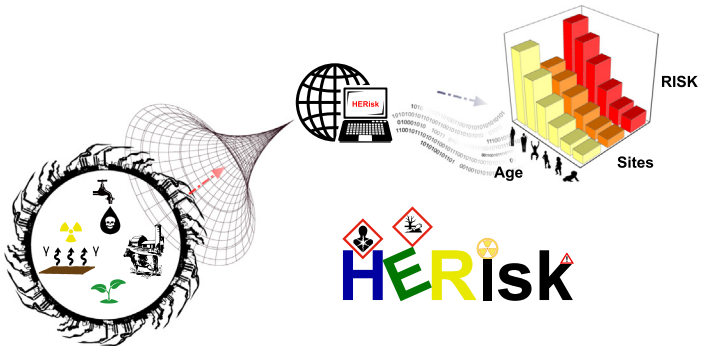

ARTICLE INFO

Article history:
Received 10 November 2020
Received in revised form 24 December 2020
Accepted 29 December 2020
Available online 2 February 2021

Editor: Filip M.G. Tack

Keywords:
Human health risk
Ecological risk
Hazardous elements
Soil & water pollution
Contaminated food ingestion

ABSTRACT

Risk assessment is considered an essential tool to assist in the management and mitigation of polluted areas, especially those associated with economic activities that significantly degrade the environment, such as mining. However, most of the methodologies of risk assessment adopt the deterministic approach of using a fixed value for ascertaining the hazards derived from exposure to chemical pollutants. However, this is not the case of the Human, Ecological and Radiological Risk (HERisk) code, which allows space-time assessments of ecological, radiological, and human health risks. Indeed, this work aims to describe this new software (enhanced version of HHRISK), which not only improves the performance of the code but also increases its applicability and versatility. To showcase its usefulness in evaluating ecological pollution and human health risk were studied the contents of potentially toxic elements (Co, Cu, Fe, Mn, Ni, Pb, and Zn) in soils and surface waters from the nickel mining area in the municipality of Itagibá (Bahia, Brazil). The obtained results showed that metals are non-homogeneous distributed, suggesting the presence of local enrichment sources, mainly related to human activities. The statistical analyses carried out revealed that mining and agricultural activities are possibly responsible for the contents of these pollutants in both soils and surface waters. The calculated ecological indices of pollution confirmed anthropogenic pollution around the mining area, especially in the locations closest to sterile waste piles. The results of the human health risk assessment revealed that the ingestion of meat and contaminated water are the main routes for entering the potentially toxic elements to the human body and that Co is the chemical specie that poses the highest risk in the entire region. The hazard index (*HI*) values indicated that the whole area around the mine should be considered as a high risk for human health.

* Corresponding author.
E-mail addresses: jordan@estudante.ufscar.br (J.B. Neris), praisegod.emenike@covenantuniversity.edu.ng (P.C. Emenike), sergiof@uesc.br (S.F.R. Andrade).

https://doi.org/10.1016/j.scitotenv.2021.145044
0048-9697/

Parameter list

ABS	Dermal absorption fraction of the chemical species
$ADAF$	Age dependent adjustments factors
AT	Averaging time (d)
BAF	Chemical species dose fraction that are absorbed by the organism (bioavailability factor)
$BW\,(i)$	Body weight for age group i (kg)
$C_f\,(t)$	Chemical species concentration in food at time t (mg kg^{-1})
$C_m\,(t)$	Chemical species concentration in the soil, sediment or water matrix at time t (mg kg^{-1} or mg L^{-1})
C_{m_ref}	Chemical species background concentration in soil, sediment or water matrix (mg kg^{-1} or mg L^{-1})
C_{TL}	Guideline value established by the national legislation (mg kg^{-1} or mg L^{-1})
C_{UCC}	Chemical species concentration in the upper continental crust (mg kg^{-1})
CF_m	Matrix contamination factor
$CR^{IA}\,(t)$	Potential carcinogenic risk at time t for initial age IA
$CR^{IA}_{agg}\,(t)$	Aggregated potential carcinogenic risk at time t for initial age IA
$CR^{IA}_{cum}\,(t)$	Cumulative potential carcinogenic risk at time t for initial age IA
CV	Coefficient of variance
$D^{IA}\,(t)$	Dose at time t for initial age IA (mg kg^{-1} d^{-1})
$D^{IA}_{ing\_f}\,(t)$	Daily intake dose of chemical species by food matrix at time t for initial age IA (mg kg^{-1} d^{-1})
ED	Number of years of exposure duration
$EF\,(i)$	Exposure frequency for age group i (d y^{-1})
$ET\,(i)$	Exposure time for age group i (h $event^{-1}$)
$EV\,(i)$	Event frequency for age group i (events d^{-1})
FI_f	Fraction ingested of contaminated food
$HI^{IA}_{agg}\,(t)$	Aggregated non-carcinogenic hazard index at time t for initial age IA
$HI^{IA}_{tot}\,(t)$	Total non-carcinogenic hazard index at time t for initial age IA
$HQ^{IA}\,(t)$	Non-carcinogenic hazard quotient at time t for initial age IA
$I_{geo}\,(t)$	Geoaccumulation index at time t for soil or sediment matrix
$IR_{ChemLoE}\,(t)$	Integrated risk for chemical line of evidence at time t
$IPI_{Th}\,(t)$	Integrated threshold pollution index at time t for soil, sediment or water matrix
$IR_f\,(i)$	Food ingestion rate for age group i (kg d^{-1})
LD	Limit of detection
$M_{d\_MPI}\,(t)$	Mean distribution coefficient Log at time t
$M.S.D.$	Standard deviation from the mean
n	Number of chemical species
PC	Dermal permeability of the chemical species (cm h^{-1})
$PERI\,(t)$	Potential ecological risk at time t for soil or sediment matrix
$PI_{nem}\,(t)$	Nemerov pollution index at time t for soil, sediment or water matrix
$PLI\,(t)$	Pollution load index at time t for soil or sediment matrix
R^2	Determination coefficient
RfD	Reference dose of the chemical species (mg kg^{-1} d^{-1})
RSD	Relative standard deviations (%)
$SA\,(i)$	Skin surface area available for contact with water or soil for age group i (cm^2)
SF	Slope factor (mg kg^{-1} $d^{-1})^{-1}$
T_r	Toxic response factor
Δt	Time variation (y)

1. Introduction

Anthropogenic activities produce tons of environmental pollutants that damage the ecosystem through the release of metal(oid)s. Industrial wastes are not left out because they constitute high amounts of pollutants often discharged into the environment without proper recovery operations nor adequate treatment (Monteiro et al., 2019). Several economic potentials, such as gains in employment and economic development, are derived through mineral resource extraction (Guo et al., 2020). However, mining actions foster environmental degradation by producing massive amounts of dust and tailings, as well as wastewater, which negatively affect air, water, and soil quality (Pokorny et al., 2019).

Many health concerns are linked to excessive intake of heavy metals, and according to the World Health Organization, children are profoundly affected than adults. Presently, epigenomic contaminants play a major part in the development of complex health cases such as metabolic syndrome, cardiovascular diseases, neurological impairments, respiratory ailments, and developing effects (Helsley and Zhou, 2017). To characterize the probability and magnitude of deteriorative health impact derived from human exposure to environmental toxicants, it is requires a multi-step procedure that incorporates scientific data to estimate the risk(s), and this assessment has been termed Human Health Risk Evaluation (HHRE). Over the years, researchers have adopted the HHRE as a verified tool for ascertaining the hazard associated with the intake or absorption of pollutants at different levels within exposed areas (Adewumi and Laniyan, 2020; Alam et al., 2020; Gyamfi et al., 2019). One significant value of the HHRE is associated with public health impact because it informs management decisions based on the available informative data.

With the rapid development of technology, computer resources and smart solutions have been created to detect zones prone to pollution and to delineate stable regions. The rationale for adopting computed software packages for risk assessments surround the occurrence of operational errors, considering that several variables are involved (Neris et al., 2019). Researchers have continually employed computer-based software such as RISC, BIOPLUME, SADA and BIOSCREEN (Newell et al., 1996; Rafai et al., 1998; Spence and Walden, 2001; Stewart and Purucker, 2006) to simulate fundamental exposure routes through which toxic chemicals reach humans. In general, these software packages have produced insightful results beneficial for HHRE, but their peculiar disadvantages lie in their inability to assess hazardous chemical exposure at variable concentration and time.

HERisk (Human, Ecological and Radiological Risk) is a unique software that incorporates a standardized technique for assessing risk in relation to all downstream activities using verified toxicological criteria outlined by the US EPA. It allows risk calculations to be tailored towards the variable exposure regime in an area while taking into account the overall aging effect of the exposed populace, giving to HERisk a greater flexibility and convenience. To this end, a more realistic assessment is achieved since the outcome is derived from an incremental effect due to chemical exposure. The uniqueness of the HERisk software hinges on its ability to provide useful information on the period when exposure will be critical. These results are essential in environmental monitoring because it provides the opportunity to swiftly mitigate pollution challenges in areas and periods where exposure levels are not critical yet. Therefore, this work aims to provide an in-depth description of the new HERisk software, as well as showcase its usefulness to evaluate the environmental impacts and human health risk associated with exposure to inorganic pollutants in a mining region.

2. HERisk software

2.1. General aspects

The HERisk software (Fig. S1, Supplementary Material) was developed to streamline and facilitate the risk calculations performance

derived from a wide range of chemical species (metal species, polycyclic aromatic hydrocarbons - PAHs, total petroleum hydrocarbons - TPHs, persistent organic pollutants - POPs, *etc.*). This new code is an enhanced version of the HHRISK (Neris et al., 2019) and, unlike other programs, it allows space-time assessments of ecological, radiological, and human health risks. This configuration allows the user to identify and assess possible threats to the environment and public health over time, as well as to assist in risk management and remediation of affected areas.

The structure flowchart of the new HERisk code is illustrated in Fig. 1. The program uses a single Excel© input file (***Input.xlsm***), which was designed to adapt the code tools to the user's interests. This file format is considered to be more interactive, facilitates the manipulation of the input data, and at the same time, creates a user-friendly interface for the new code.

This file is divided into several sheets, which includes (i) the number of chemical species and their concentrations in each matrix studied (ii) the number of locations and times considered in the analysis, as well as the values of the exposure time parameters. In this file, different buttons (logic keys) were created to choose the exposure pathways, the scenario, the exposure type and the risk assessments that the user wants to consider (see Fig. S2, Supplementary Material).

This input file also contains the ***Dataecological*** and ***Datachemical*** sheets, which are databases storing the reference values provided by human health and environmental protection agencies. Any chemical species whose parameters and reference values were previously defined by the responsible institutions can be added to these databases.

As shown in Fig. 1, all values contained in the input file are read and stored by the program *via* the ***Readinput*** subroutine. Based on this information, the code performs calculations corresponding to the type of risk assessment requested by the user. For the HHRE, three main subroutines are used: ***Exposure***, ***Riskag***, and ***Riskcum***. The ***Exposure*** subroutine coordinates the first part of the process, selecting the activated pathways and the parameter values related to the chosen scenario and using the ***Doseways*** subroutines (1 to 14) to perform the doses and individual risks calculations (*D*, *HQ*, *CR*). Then, the ***Riskag*** and ***Riskcum*** subroutines calculate the leading indices used in health risk assessment, such as HI_{agg}, HI_{tot}, CR_{agg}, and CR_{cum}. The parameters calculated in these routines are displayed to the user in 6 output files (see Fig. 1).

This code includes two new routines: ***Radio_risk*** and ***Ecol_risk***, created to assess radiological and ecological risks. As shown in Fig. 1, ***Radiological_Risk.out*** is the only output file associated with the radiological risk routine, while the calculations performed by ***Ecol_risk*** are shown in two separate files: ***Ecological_Risk_Individual.out*** and ***Ecological_Risk_Combined.out***. The indices calculated in the ***Ecol_risk*** routine will be described in the next section, while the ***Radio_risk*** routine will be described in greater detail in a future work.

In general, the program computation does not exceed 3 s, which makes HERisk a very useful tool to perform radiological, ecological, and human health risk assessments extremely quickly and accurately. Precisely, the accuracy of the risk assessment calculations was tested, comparing the results obtained with those reported in similar published studies (Table S1). It is worth mentioning that in all cases, the percentage deviation values did not exceed 0.7%.

More detailed information about other features of the code, as well as the methodology used to calculate the uncertainties can be found in Neris et al. (2019). Before proceeding with the description of the main parts of the code, it is worth mentioning that all the equations implemented in HERisk are listed in the supplementary material (Table S2).

2.2. Human health risk assessment

The human health risks assessment can be conducted using three possible scenarios: agricultural, industrial, and residential, which consider specific routes and exposure parameters for each of them (Neris et al., 2019). Depending on the selected scenario, the code calculates the health risks through 14 different exposure routes: 10 associated with soil, water or food (meat, milk, eggs, vegetables, fruits, and grains) ingestion, 2 associated with inhalation (particulate matter or gases), and 2 for dermal contact (soil or water).

HERisk differentiates the outcome of the risk assessment in two categories as defined by the US EPA (1989), non-carcinogenic risks with non-cumulative effects and carcinogenic risks with cumulative effects. The code uses the formulas provided by the US EPA (2009, 2004, 1989) with some adjustments to perform the spatio-temporal risk assessment (Neris et al., 2019). The use of US EPA equations as a basis for HERisk methodology led to some limitations for this new approach, which are the same as conventional methods. Among them are the need and availability of a significant set of essential parameters used in the risk assessment process. Despite this, the software has no restrictions on the number of chemical species, locations, or times for which simultaneous risk calculations can be performed.

This methodology starts with calculating the daily intake dose and the daily absorbed dose, which represents the quantity of the contaminant that enters the organism through ingestion and dermal routes, respectively. These quantities depend on intrinsic chemical species parameters (Concentration, *PC*, *ABS*), exposure duration parameters (*EF*, *EV*, *ET*, *etc.*) and physiological parameters (*BW*, *IR*, *SA*, *etc.*) as shown in Eq. (1), used to calculate the contaminant daily intake doses by food ingestion. The doses equations for the other exposure routes are described in Eqs. ((S1)–(S5)) in the supplementary material.

$$D_{ing\_f}^{IA}(t) = \sum_{t=\Delta t}^{ED} \frac{C_f(t)\cdot IR_f(i)\cdot FI_f\cdot EF(i)\cdot \Delta t}{BW(i)\cdot AT} \quad (1)$$

Depending on the duration and frequency of the residents' exposure to pollutants, the risk can be classified as acute, subchronic, and chronic. The HERisk configuration considers an exposure of up to 14 days as acute, from 15 to 364 as subchronic and greater than 365 days as chronic (ATSDR, 2018).

Since constant human development results in severe physiological and dietary changes; it is necessary to perform HHRE considering this variation. In this new program, the ***Redistribution*** subroutine was implemented to give a more realistic spatio-temporal risk assessment by including age-dependent parameters for the different stages of human development. Based on the US EPA (2011) guideline and data provided by the Brazilian Institute of Geography and Statistics (IBGE), the code allows supplying different values for the age-dependent parameters for the following age groups (i): 1 to <2 years ($i = 1$), 2 to <3 years ($i = 2$), 3 to <6 years ($i = 3$), 6 to <11 years ($i = 4$), 11 to <16 years ($i = 5$), 16 to <18 years ($i = 6$), 18 to <21 years ($i = 7$), 21 to <65 years ($i = 8$) and >65 years ($i = 9$).

Since age-dependent parameters vary over time and assume values depending on the human's age group, it is necessary to know the initial age at which residents begin to be exposed to contaminants. The current program performs the calculations of the human health risks for nine initial ages ($IA = 1, 2, 3, 6, 11, 16, 18, 21$ and 65 years), separately. Therefore, the program calculates the risk considering that exposure can start at different life stages, which allows us to perform risk calculations more realistically.

In the specific case of the dose calculation by food intake (Eq. (1)), the code allows to carry out the risk assessment without necessarily having to know the concentration of the contaminants in food. The program uses equations (Eqs. (S6)–(S10)) provided by Health Canada (2005) to model the transport of contaminants present in environmental matrices to the biological receptors that form part of the human food chain.

Once the doses for each exposure pathway and chemical species are known, the potential carcinogenic risk (*CR*) and the non-carcinogenic hazard quotient (*HQ*) are calculated. A novelty of the current code is the inclusion of the bioavailability factors (*BAF*) and the age-dependent adjustment factors (*ADAF*) in the calculation of these indices (Eqs. (2)–(3)), as recommended by the US EPA (2007, 2005). *BAFs* allow

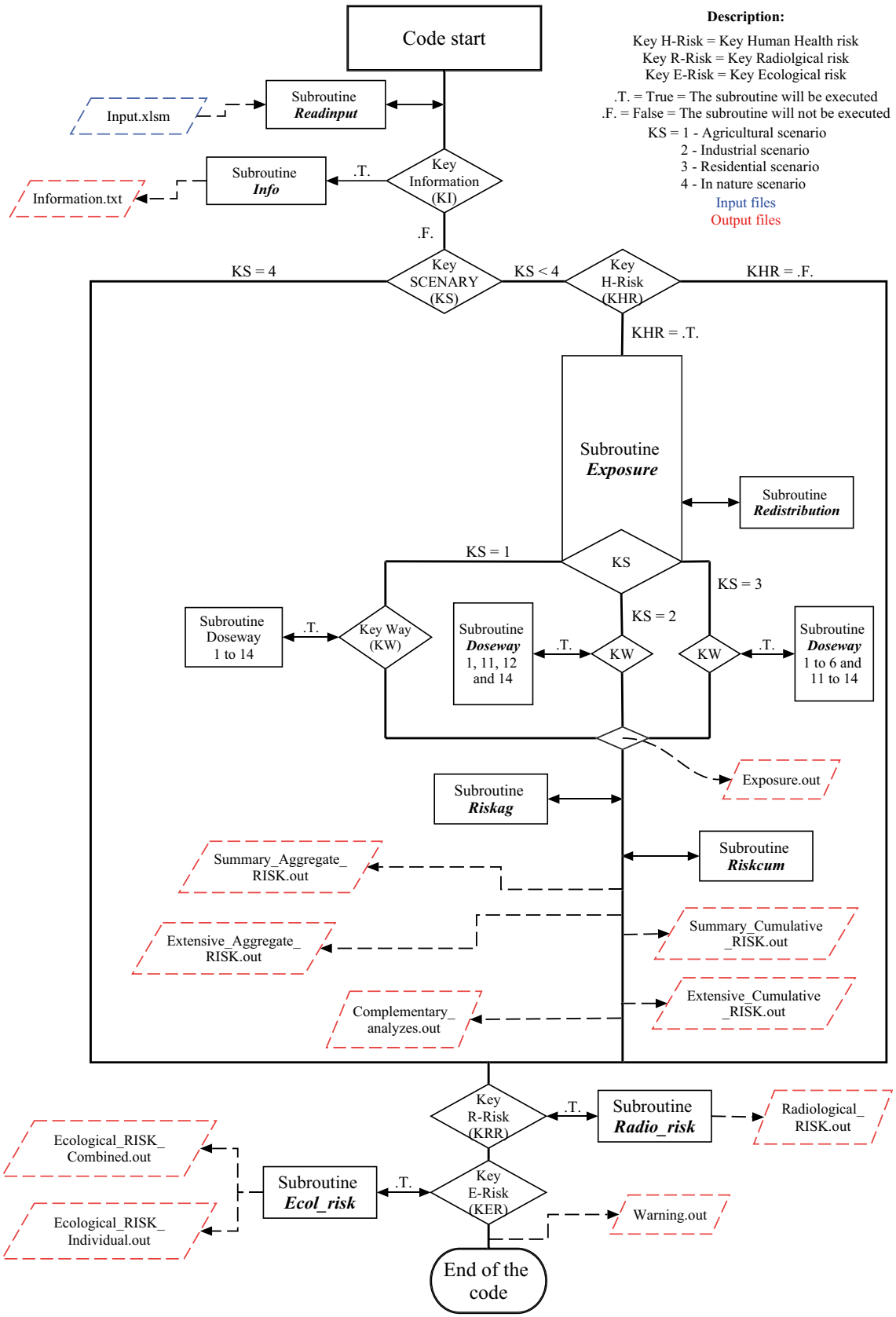

Fig. 1. Flowchart diagram of the HERisk code.

defining the chemical species dose that is absorbed by the human body, while *ADAFs* are applied when a carcinogenic species has mutagenic modes of action.

$$HQ^{IA}(t) = \frac{D(t)\cdot BAF}{RfD} \quad (2)$$

$$CR^{IA}(t) = D(t)\cdot SF\cdot BAF\cdot ADAF \quad (3)$$

This subroutine uses the ***Datachemical*** database, where are stored the *RfD*, *SF*, and *BAF*, which were taken from: US EPA, ATSDR, Health Canada, OEHHA and from a vast bibliographic review (Fairweather-Tait and Hurrell, 1996; Hu et al., 2013, 2011; Leggett, 2008).

Once the HHRE is carried out considering various exposure routes, it is necessary to calculate the aggregated risk index (HI_{agg}) and the potential aggregated cancer risk (CR_{agg}) (see Eqs. (S11)–(S12), Supplementary Material). These indices provide the sum of non-carcinogenic (*HQ*) and carcinogenic risks (*CR*) resulting from multiple exposure pathways. Finally, to obtain the overall risk incorporating all exposure routes and all chemical species, the code calculates the total risk index (HI_{tot}) and the potential cumulative carcinogenic risk (CR_{cum}) (see Eqs. (S13)–(S14), Supplementary Material).

2.3. Pollution and ecological risk assessment

The ***Ecol_risk*** subroutine was implemented to assess the environmental pollution level and the possible toxic effects on organisms resulting from the chemical species concentration in environmental matrices of the studied areas. Since ecological studies often are focusing on uninhabited regions, this code includes a new scenario called "*In Natura*." This scenario considers that the contaminated area evaluated is deprived of inhabitants, but not necessarily free from human activities. It can be used to investigate the natural occurrences of harmful chemical species in the studied areas and to assess the ecological risks resulting from anthropogenic activities. The ***Dataecological*** database stores the reference or background values (C_{m_ref}, C_{TL}, C_{UCC}, *etc.*) used for the ecological indices calculation. This modifiable database allows the choices of guidelines values established by regional, national, or international environmental legislation.

The ecological risk assessment methodology adopted in the HERisk is the result of a vast bibliographic review, which includes among other relevant works the followings: Jensen et al. (2006), Pagliarini et al. (2019) and Hakanson (1980). Among all indices reported, the 15 most used were included in the code.

Pollution indices were grouped into three different categories: single, combined, and integrated. Single indices, such as the contamination and the enrichment factors, assess the pollution arising from individual chemical species based on their concentrations and the reference values provided in the database (see Eqs. (S16)–(S20)). The pollution load index (*PLI*, Eq. (4)) and the integrated threshold pollution index (IPI_{Th}), among other combined indices included in the code, are calculated based on the single indices and serve to assess the degree of contamination in different matrices due to the simultaneous presence of numerous chemical species (see Eqs. (S21)–(S27), Supplementary Material).

In addition, the code evaluates the toxicity effect of the chemical species on the living organisms of a given ecosystem. With this purpose indices such as the potential ecological risk index ($PERI_m$, Eq. (5)), the toxic risk index (*TRI*), among others are included in the code to inform the ecological vulnerability of the studied area (Emenike et al., 2020).

$$PLI_m(t) = \sqrt[n]{\prod_{j=1}^{n} CF_m^j(t)} \quad (4)$$

$$PERI_m(t) = \sum_{j=1}^{n} T_r^j \cdot CF_m^j(t) \quad (5)$$

The integrated indices (Eqs. (S28)–(S33), Supplementary Material) give a comprehensive expression for analyzing the interrelationships between the different matrices and characterize the risk value of the studied location by using a single index. This third group includes two leading indices: the mean distribution coefficient Log (M_{d_MPI}) and the integrated risk for the chemical line of evidence ($IR_{ChemLoE}$). The $IR_{ChemLoE}$ allows evaluating the extent of the ecological risk by using the substance-based approach that compares the total concentrations of each pollutant at the study sites with individual screening values reported for each matrix, which is known as Chemical Line of Evidence (ChemLoE) (Son et al., 2019).

3. Materials and methods

3.1. Description of the study area

The present study was carried out in the nickel mining area, belonging to the municipality of Itagibá (Bahia, Brazil). The region is characterized by an average annual temperature that varies between 22 and 26 °C. The annual precipitation is approximately 1100 mm, with 85% relative humidity. The season with the highest precipitation lasts approximately eight months, from November to July. The months of August to October are the driest.

The Santa Rita mine is the third largest open-pit nickel sulfide mine in the world, with a volume of exploitable ores of approximately 167.8 Mt (CBPM, 2009). The mine has been operational since April 2009 and is located on the "Santa Rita" farm, in an area of approximately 10 km^2 and 50 to 400 m wide (Barnes et al., 2011). The mine operations were halted in 2016 due to macroeconomic conditions and resumed since the end of 2019. Besides, according to CBPM (2020), the mine operation can be extended for more than 20 years.

Approximately 83% of the extracted rocks are discarded as sterile with the possibility of generating acid drainage. The sterile piles are left close to the pits with no specific destination (RIMA, 2006). The tailings are pumped through the processing plant piping to the tailing basin in pulp form with about 55% solids and 45% aqueous solution (RIMA, 2006). Besides, on the west side of the mine is the Oncinha stream, and to the east is a dense water resources system formed by the Contas, Formiga, and the Peixe rivers (Fig. 2). These rivers are mainly used for agricultural and livestock activities by the local population.

The mine also indirectly affects an area of approximately 480 thousand ha, which are used by residents (population: 14,579) for livestock, cocoa, and horticulture activities (IBGE, 2019). Also, in this region, located between the cities of Ipiaú and Itagibá (State of Bahia), there are several farms producing cocoa, banana, cassava, beans, corn, orange, and sugar cane (RIMA, 2011, 2006).

3.2. Samples collection and analysis

Surface water and soil samples were collected at five different sites around the "Santa Rita" mine. The sample collection was carried out using a semicircular sampling scheme respecting the mine outline, with a distance between 500 and 700 m from the main pit center (CETESB, 2001). These sampling points were chosen due to their critical locations and for being the most susceptible to ecological and human health risks, as they are close to the tailing piles, main water sources, and populated areas. In Fig. 2 and Table S3 are presented the georeferenced sampling points (P01–P05). The collection occurred in the dry season, specifically in August, for three consecutive years.

The soil samples collection was performed, removing approximately 3 kg per collection at a depth of 20 cm, with 3 replicates. The samples were identified and packed in impermeable plastics to conserve natural moisture. In the laboratory, soil samples were initially dried in an oven (Marte Científica) 100 ± 2 °C to reduce humidity. A portion of each

sample was ground in a porcelain mortar and sieved with 360 mesh size. Subsamples of 0.25 g were added in a digestion tube with 2.5 mL HNO_3 (Merck, 68%) and 1.5 mL HCl (Merck, 37%). The resultant samples were placed in the digester block and heated at 120 °C for 2 h. Finally, the samples were left at room temperature, completed with 15 mL of ultrapure water Milli-Q (Merck group) and centrifuged at 2000 rpm for 5 min (Solab Científica, model SL-700) (U.S. EPA, 1994a).

The surface water samples were collected in the water column corresponding to the fine sediment deposition in the riverbed, as recommended by CETESB-ANA (2011). The samples were stored at 4 °C in glass containers (500 mL) of inert material with waterproof covers. For the proper water samples conservation and to avoid the precipitation and adsorption of inorganic species on the container walls, was added 1 mL of HNO_3 solution (10% v/v).

As recommended by CETESB-ANA (2011), before acid digestion, surface water samples were filtered using a microfiltration membrane (0.45 μm pore size) for sieving colloidal particles and suspended material. A representative 10 mL aliquot of each water sample was added to a digestion tube with 0.20 mL HNO_3 and 0.10 mL HCl, as recommended by ISO (1995) and U.S. EPA (1994b). The samples were subsequently heated in a digester block at 85 °C for 3 h and kept under reflux. After acid digestion, the samples were cooled, transferred to Falco tubes (50 mL) and added 15 mL of ultrapure Milli-Q water. The resulted samples were centrifuged at 2000 rpm for 5 min.

To determine the metals Co, Cu, Fe, Mn, Ni, Pb and Zn in the water and soil samples was used an atomic absorption spectrometer SpectrAA 240FS (Varian). The calibration curve presents linearity up to 50 mg L^{-1} and the determination coefficients (R^2) for all metals exceeded 0.9900. Samples with concentrations greater than 50 mg L^{-1} were diluted with ultrapure water. All samples were measured in triplicate, and the relative standard deviations (*RSD*) did not exceed 10%. The limit of detection (*LD*) for each element was determined from ten analytical blanks prepared using ultrapure Milli-Q deionized water and under the same analytical conditions as the samples.

3.3. Statistical analysis

The dataset obtained was analyzed in terms of classic parameters of descriptive statistics such as minimum and maximum values, mean, standard deviation from the mean (*M.S.D.*), skewness and kurtosis.

Multivariate analyzes such as Spearman's correlation coefficient and Hierarchical Cluster Analysis (HCA) were performed using the STATISTICA 10 software. Spearman's correlation, at the significance levels of $p < 0.05$ and $p < 0.01$, was used to find the relationships between the pollutants and to determine possible pollution common sources. In the case of HCA, the Euclidean distance was used as a similarity measure associated with the metal origins in the samples.

3.4. Methodology for risk assessment

In this study, seven chemical species (Co, Cu, Fe, Mn, Ni, Pb, and Zn) were considered to carry out the ecological and human health risk assessments. For the CF_{soil} and I_{geo} calculations were used the regional background values defined by Biondi et al. (2011) and da Silva et al. (2015), while for CF_{water} the national reference values defined by CONAMA (2005). Likewise, for calculating the IPI_{Th} for soil and water matrices, limit values stipulated by Brazilian legislation through CONAMA 420/2009 and CONAMA 357/2005 Resolutions were used, respectively (CONAMA, 2009, 2005).

The health risk assessment was estimated for an agricultural scenario by evaluating seven routes of human exposure to contaminants (Eqs. (1) and (S1)–(S4), Supplementary Material). The pathways associated with soil (accidental ingestion and dermal contact) and the consumption of contaminated foods were considered as chronic exposure routes, whereas accidental ingestion and dermal contact with water during swimming were considered acute exposures.

Since the region studied has an intense agricultural activity, with banana, orange, guava, avocado, coconut, beans, manioc, meat, and bovine milk as representative cultures, the risks associated with the consumption

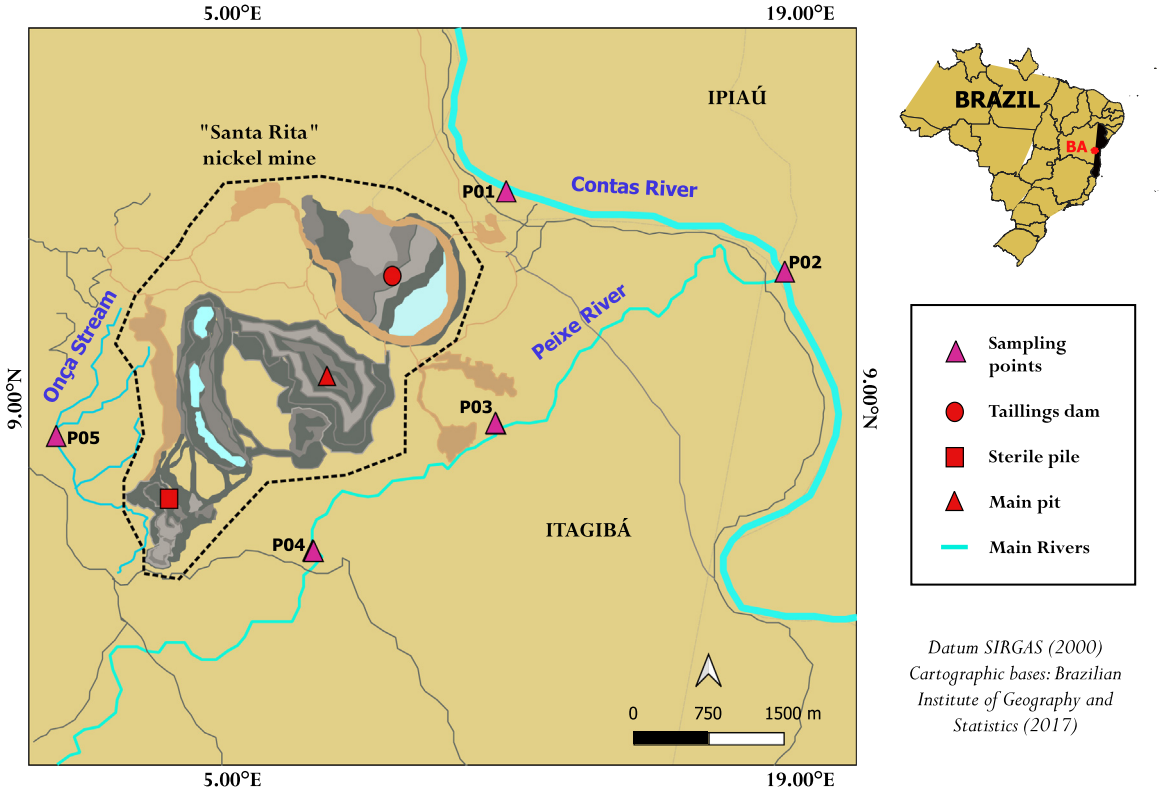

Fig. 2. Map with the sampling points locations around the nickel mine "Santa Rita", Itagibá-BA/Brazil.

of these foods were considered in the human health risk assessment. The chemical species concentrations in these foods were estimated using Eqs. (S6)–(S10).

The human health risk was assessed considering an exposure time of 20 years following the "Santa Rita" mine operating plans. During the first three years of exposure, the experimental concentrations found in surface water and soil matrices were utilized, while for the other years, the averages values of the experimental concentrations of each metal at each point were used. This approximation provides a human health risk estimative during all 20 years of the mine operation.

The carcinogenic and non-carcinogenic risks with their uncertainties were obtained through Eqs. (3)–(4) and (S11)–(S14). All the parameter values used for the risk calculations are presented in Tables S4–S9 and were extracted mainly from data provided by IBGE and CETESB (Environmental Company of the State of São Paulo). The non-carcinogenic risk values were classified according to U.S. EPA (1989) criteria: negligible ($HI_{tot} < 0.1$), low ($0.1 \le HI_{tot} < 1.0$), medium ($1.0 \le HI_{tot} > 4.0$) and high ($HI_{tot} \ge 4.0$), while according to Li et al. (2014) the carcinogenic risk is negligible when the probability of a resident developing cancer is less than 1 in 1,000,000 ($CR_{cum} < 1 \cdot 10^{-6}$), low when $1 \cdot 10^{-6} \le CR_{cum} < 1 \cdot 10^{-4}$ and high when $CR_{cum} \ge 1 \cdot 10^{-4}$. The classification of ecological risks and environmental pollution are shown in Table S10 of the supplementary material.

4. Results and discussion

4.1. Concentration of potentially toxic elements (PTE) in soil and surface water samples

The descriptive statistical analysis associated with concentrations of PTE (Co, Cu, Fe, Mn, Ni, Pb, and Zn) measured in the samples and their permissible values endorsed by Brazilian environmental law in the soil and surface water are summarized in Table 1. For more detailed information of the concentration values specified by sampling location (see Tables S11–S12, Supplementary Material).

The average metals concentrations in soils decreased in the following order: Fe > Mn > Ni > Co > Cu > Zn > Pb. The highest average concentration values were for Fe (176 mg kg^{-1}), and Mn (125 mg kg^{-1}), which is an expected result since both metals are among the most abundant elements in soils (Railsback, 2003). On the other hand, Zn and Pb exhibited the lowest concentrations for all sites, with an average of 1.29 mg kg^{-1} and 0.85 mg kg^{-1}, respectively. The coefficient of variance (*CV*), which indicates the degree of variability within the metal concentrations spectrum, ranged between 50% and 100%. This reflects a non-homogeneous distribution of the metals, which suggests the presence of local enrichment sources, mainly related to human activities (Doabi et al., 2018).

The high positive skewness and kurtosis values for Cu, Pb, and Zn (see Table 1) indicate a right-skewed and leptokurtic distribution. In the case of Co, Fe, and Ni, they follow a right-handed and platykurtic distribution, indicating that extreme values have low probabilities. The skewness and kurtosis of Mn suggest that it is the only element in soil samples that can be considered normally distributed.

In general, the highest metals concentrations in soils were identified in the sampling points: P03, P04, and P05, which are the closest to the mining area. In P03 the maximum concentration values of Co (19.3 mg kg^{-1}), Ni (17.2 mg kg^{-1}), Pb (2.98 mg kg^{-1}), and Zn (7.45 mg kg^{-1}) were observed; whereas P04 showed the maximum concentrations of Cu (33.9 mg kg^{-1}) and Fe (359 mg kg^{-1}). In addition, high values of Co, Mn, and Ni were confirmed for this point. In the case of P05, not only was the maximum concentration of Mn (216 mg kg^{-1}) found but also high Fe and Pb concentrations.

Although the concentration values did not exceed the permissible values established by CONAMA (2009), it is worth mentioning that the mean values of Co and Ni did exceed regional background values of 3.1 mg kg^{-1} and 7.6 mg kg^{-1}, respectively. Furthermore, in some specific sites during the three sampling campaigns, Mn concentrations were observed above the regional background level: 186 mg kg^{-1} (P01-first campaign) and 216 mg kg^{-1} (P05-third campaign). Likewise, the Cu concentration (33.9 mg kg^{-1}) found in P04 (third campaign) surpassed the regional value, as well as the value for the Upper Continental Crust (28 mg kg^{-1}) (Rudnick and Gao, 2014).

For surface water samples the total average concentrations followed a decreasing order similar to that observed for the soil samples, except for Co that ranked third (Table 1). Fe and Mn showed extremely variable concentration values with *CV* values of 82% and 92%, respectively. According to the skewness and kurtosis, Fe follows a normal distribution, while for Mn, they represent a right-skewed and leptokurtic distribution. All locations exhibited Fe and Mn concentrations that exceeded the permissible limits recommended by Brazilian law (CONAMA, 2005).

The Co and Ni concentrations in surface waters presented a similar behavior. Neither Co nor Ni concentrations followed a normal distribution. 93% of the samples surpassed the safe limits values for both metals in all locations. In the case of Cu, it was only detected in two sampling points (P01 and P04) in different campaigns, and the detected concentrations were higher than the CONAMA stipulated threshold.

Zn and Pb were the least abundant metals with average concentrations of 0.64 mg L^{-1} and 0.60 mg L^{-1}. Their concentrations followed opposite distributions: a right-skewed leptokurtic distribution for Zn and a left-skewed platykurtic distribution for Pb. The highest Zn concentration (1.45 mg L^{-1}) was identified in P05, while P01 showed the maximum concentration of Pb (1.05 mg L^{-1}). During the three sampling campaigns in all the five locations studied, concentrations of both metals exceeding the CONAMA limits were detected.

In general, the obtained values show possible contamination of the regional water resources, since the average concentrations for all metals are at least three times greater than the permissible values. Likewise, the average concentrations (except Cu and Zn) are above the safe values proposed by the Initiative for Responsible Mining Assurance (IRMA, 2018).

These preliminary results indicate a possible impact on both the soils and water resources associated with mining activity in the region. The high PTE concentrations observed, especially at sampling points P03–P05, could probably be caused by ores processing activities and the presence of the sterile waste piles, which are located close to these sites.

4.2. Statistical analyses: identification of pollution sources

The Spearman's correlation and HCA were used to identify interrelationships among the different metals, as well as common pollution sources. The Spearman's correlation coefficients (r_S) for metals in soil and surface water samples are shown in Table S13 of the supplementary material.

In the soil samples collected in the mining area, a strong positive correlation at a significance level $p < 0.01$ was observed between Co and Ni ($r_S = 0.9068$). Likewise, both metals showed moderate positive correlation with Cu (Co-Cu: $r_S = 0.5806$ and Cu-Ni: $r_S = 0.5795$, $p < 0.05$), thus indicating a common origin for these three elements. Economic concentrations of nickel-bearing minerals occur as sulphides and in laterites (BGS, 2008). Since the "Santa Rita" nickel mine is one of the largest open-pit nickel sulphides mines; minerals such as pentlandite ($[Fe, Ni]_9S_8$), siegenite ($[Ni, Co]_3S_4$) and carrollite ($Cu\,[Co, Ni]_2S_4$) can be found forming part of the regional rocks (Atlantic Nickel, 2020). In the study conducted by Da Matta (2016), some of the inference highlighted that: (1) the solid wastes from "Santa Rita" mine contain high concentrations of oxides of iron and traces elements like Co, Cr, Cu, Ni, Ti, and V; (2) rocks in the sterile wastes piles are highly susceptible to weathering. Additionally, it has been reported that fractions of Co, Cu, and Ni may be removed from solid wastes by leaching process carried out by bacteria under atmospheric pressure and normal temperature condition (BGS, 2008). Based on these facts and considering the proximity of the sampling points to the sterile waste piles, the contents of Co,

Table 1
Descriptive statistics of total PTE concentrations in soil and water samples from the mining area.

Soil (mg kg^{-1})	Co	Cu	Fe	Mn	Ni	Pb	Zn
Range	1.63–19.3	0.10–33.9	14–359	9–216	2.00–17.1	<LD–2.98	0.19–7.45
Median	4.59	1.35	161	133	5.80	0.71	0.52
Mean	7.63	3.43	176	125	7.69	0.85	1.29
M.S.D.	1.72	2.44	30.6	14.5	1.45	0.23	0.58
CV (%)	80	97	67	52	69	96	98
Skewness	1.01	3.84	0.69	−0.59	0.74	1.80	2.55
Kurtosis	−0.57	14.8	−1.37	−0.42	−1.01	3.11	6.17
Permissible Value [a]	25	60	-	-	30	72	300
C_{ref} [b]	3.1	5.9	-	173.4	7.6	19.5	45.4

Water (mg L^{-1})	Co	Cu	Fe	Mn	Ni	Pb	Zn
Range	0.03–7.93	<LD–1.05	2–423	<LD–33.0	0.03–3.62	0.03–1.05	0.21–1.45
Median	1.54	0.67	151	1.02	1.00	0.73	0.62
Mean	2.33	0.67	164	6.10	1.42	0.60	0.64
M.S.D.	0.54	0.39	33.5	3.04	0.27	0.08	0.08
CV (%)	85	82	82	92	68	52	57
Skewness	1.81	-	0.52	2.07	1.13	−0.66	1.38
Kurtosis	3.84	-	-0.41	3.80	0.86	−0.95	3.28
Permissible Value [c]	0.05	0.01	0.3	0.1	0.03	0.01	0.18
Permissible Value [d]	-	1.0	0.3	0.1	0.04	0.01	3.0

LD: limit of detection.
[a] CONAMA (2009).
[b] C_{ref}: Regional background concentration of metals (Biondi et al., 2011; da Silva et al., 2015).
[c] CONAMA (2005).
[d] IRMA (2018).

Cu, and Ni found in the soils can be attributed to the mining activity within the region.

A strong positive correlation was also observed between Fe and Mn ($r_S = 0.8178$, $p < 0.01$). Despite most of the nickel-bearing minerals and the solid wastes associated with nickel processing contain high concentrations of Fe (up to 12%), the leaching efficiency of Fe is lower compared to that of other metals such as Ni, Cu, and Co (Xie et al., 2005). Furthermore, Mn content in sterile waste piles is much less than 1% (Da Matta, 2016). This might be the reason why neither Fe nor Mn exhibited significant correlations with those metals. It is noteworthy to mention that nickel sulphides minerals in economic deposits occur in mafic and ultramafic rocks, which are iron-rich igneous rocks and also have high contents of Mn (BGS, 2008). For this reason, the high concentrations of both metals found in soils may be linked to a geogenic source.

Finally, Pb and Zn were highly correlated ($r_S = 0.7756$, $p < 0.01$). Since these elements showed negative correlations with Fe and Mn, they are not associated with natural sources. However, they exhibited weak correlations ($0.0071 \le r_S \le 0.4588$) with the other metals, which indicates that they have an anthropogenic origin different from mining activities. Phosphate fertilizer application and animal manure are responsible for increasing the levels of Pb and Zn in soils (Marrugo-Negrete et al., 2017). Therefore, the presence of these metals in soils can be associated with agricultural and livestock activities taking place within the region.

In the case of the surface waters, Cu was not included in the statistical analyses because it was only detected in 13% of the samples. The highest positive correlation was observed for Co and Ni ($r_S = 0.7171$, $p < 0.01$). Both metals were also moderately correlated with Mn (Co-Mn: $r_S = 0.6296$ and Mn-Ni: $r_S = 0.6877$, with $p < 0.05$). This could be associated with the presence of aplowite [$(Co, Mn, Ni)SO_4 \cdot 4H_2O$], a tetrahydrate mineral that may occur in cobalt- and nickel-bearing sulphides deposits (Mindat.org, 2020). However, it has been reported that this metal association is commonly found in polluted aquatic environments, where the excess of Co, Mn, and Ni tends to merge around small fragments of debris and organic materials (BGS, 2008). For that reason, there is a high possibility that mining may adversely affect these resources, given the proximity of the sterile waste piles to the water bodies.

Pb was negatively correlated with Mn ($r_S = -0.6645$, $p < 0.01$) and Co ($r_S = -0.6368$, $p < 0.05$), while showed a moderate positive correlation with Zn ($r_S = 0.6239$, $p < 0.05$). The association among these pollutants reinforces the hypothesis that both Pb and Zn emanate from anthropogenic activity other than mining, such as agriculture.

The dendrograms of metal concentrations in soil and water samples obtained from HCA are presented in Fig. 3. In general, HCA identified two main clusters that confirmed the interrelationships among PTE. The first one includes Fe and Mn (for soil samples) and only Fe (for surface waters), which suggest that the high content of these metals could originate from natural (lithogenic) sources. The second cluster for soil samples is formed by two groups (Co-Ni and Pb-Zn) and Cu, which are metals mainly produced by anthropogenic sources, such as mining and agriculture. The fact that Cu is associated with both groups suggests that its presence in regional soils is not only associated with mining, but also with agricultural activities. In the case of surface waters, the second cluster includes Co, Mn, Ni, Pb, and Zn. As was mentioned, mining and agricultural activities may be responsible for the loading of PTE entering regional water sources.

4.3. Pollution level and ecological risk assessment

From the determined concentration of PTE in soil and water samples, both single and combined pollution indices were calculated.

The *CF* values in soils are summarized in Fig. S3a. In the soils, the *CF* range for each metal was: Co (0.47–5.51), Cu (0.02–5.72), Fe (0.001–0.022), Mn (0.05–1.25), Ni (0.26–2.25), Pb (0.001–0.153) and Zn (0.004–0.164). Based on the total *CF* average values, soils exhibited moderate pollution only for Co and Ni ($1 \le CF < 3$). In four locations (80%), the *CF* values for Co indicated contamination by human sources ($CF > 1$). P01 and P02 showed a moderate pollution level, while P03 and P04 exhibited heavy contamination ($3 \le CF < 6$). These last two points also showed moderate pollution of Cu and Ni. Finally, in P05, Mn exhibited moderate pollution. As can be noticed, the sampling points closest to the sterile waste piles were the most contaminated.

The negative values of I_{geo} obtained for Cu, Fe, Mn, Pb, and Zn corroborated that there is no level of contamination of these metals in the soils of the studied area. Again, Co showed the highest accumulation in the

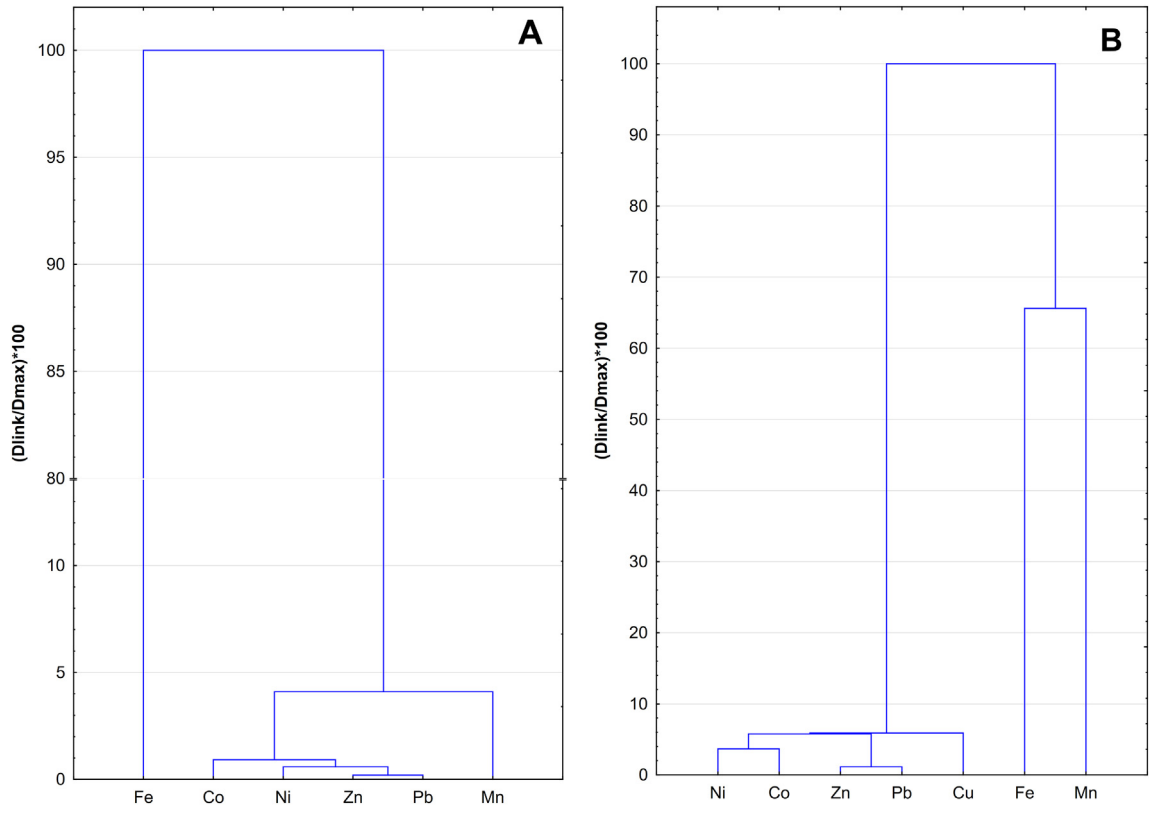

Fig. 3. Dendrograms obtained *via* HCA of metal contents in (A) surface waters and (B) soil.

soils, specifically in P03, where its I_{geo} value (1.15) revealed moderate pollution ($1 \leq I_{geo} < 2$).

The *CF* values based on the guideline values of CONAMA for all metals in surface waters are shown in Fig. S3b. The total *CF* average for each metal was: Co (48.9), Cu (9.85), Fe (547), Mn (52.9), Ni (56.8), Pb (60.5), and Zn (3.53). As can be noticed, all the metals (except for Zn) showed severe contamination ($CF > 6$). Therefore, all the locations (100%), where these metals were detected, can be classified as extremely polluted, indicating the severe impact of human activities on water resources. 80% of the sampling points showed heavy pollution ($3 \leq CF < 6$) for Zn.

The mean of the combined indices *PLI* (0.15), mC_d (0.66), IPI_{Th} (0.07), and PI_{Nem} (0.36) revealed a very low degree of contamination in the soils of the total studied area. Again, P04 was the most polluted location by showing the maximum values of mC_d (1.84) and PI_{Nem} (0.90), which means the level of pollution in this site can be considered as low to moderate, within the warning limits (see Table S10, Supplementary Material).

A different picture was observed for surface waters. The R_{W_comb} reached the maximum value of 1 for all locations. In addition, *PLI* for surface waters was over 1 (mean: 39.4) and varied from 13.3 to 86.7. The IPI_{Th}, ranged within the interval 24.6–244, and the mean value was 111. In general, all these indices indicated that water resources could be classified as extremely polluted.

The Ecological risk was assessed by using *PERI* values, which in soils varied from 6 to 61, with a mean value of 19.8. These results revealed a low ecological risk ($PERI \leq 90$). On the other hand, *PERI* values in surface water ranged from 302 to 1844, with an average of 936 (extremely ecological risk). In the total area: 7% of the sites were between 180 and 360 (strong ecological risk), 13% were between 360 and 720 (very strong ecological risk), and 80% of the values were above 720, indicating a highly strong ecological risk. Fig. S4 shows the average values of IPI_{Th} and *PERI* indices in each sampling point. According to the results, the sampling points P03 and P04, which are the ones with closet proximity to sterile waste piles, exhibited the highest values for these indices, and therefore, are the most impacted by the mining activity.

4.4. Human health risk assessment

Three main indices were used to assess the human health risk: HI_{agg}, HI_{tot}, both for evaluating the non-carcinogenic risk; and the CR_{cum} for carcinogenic risk.

Fig. 4a shows that HI_{agg} values for total area decreased in the following order: Co > Ni > Fe > Mn > Cu > Pb > Zn. As can be noticed, Co is the metal that exhibited the highest HI_{agg} values, ranging from 2.5 to 5.3, indicating that the concentrations found for this metal pose a moderate to high risk to human health, especially in P03 and P04 locations. For Fe and Ni the values were below 1, which suggests low risk. Since the HI_{agg} values of Cu, Mn, Pb and Zn for all locations were lower than 0.1, no non-carcinogenic risks are associated with these metals.

Fig. 4b shows a similar analysis but from the perspective of the HI_{agg} associated with each metal and age range. Again, Co is the largest contributor to the total HI_{agg} value for all age groups. For children up to the age of 16, more than 82% of the aggregate hazard index is attributed to cobalt. Meanwhile, for those over 18 years, it represents approximately 77%. Ni is the second chemical species that contributes the most to total HI_{agg}, with a growing influence throughout human development. For all the age ranges, Fe contribution remained relatively constant with an approximate value of 9%.

Based on the results obtained with the HERisk program, it was possible to identify that the ingestion of PTE is the main exposure route that threatens human health (Fig. 4c). For all age groups, the meat consumption accounts for most of the total risk (over 57%), especially in children up to the age of 16, where the mean value was 67.2%. Fresh milk consumption was the second route of dietary exposure (the third in total) that most contribute, representing between 5.8% and 9.6% of the HI_{tot}. The highest value was observed for the youngest ($1 < 2$) and the lowest

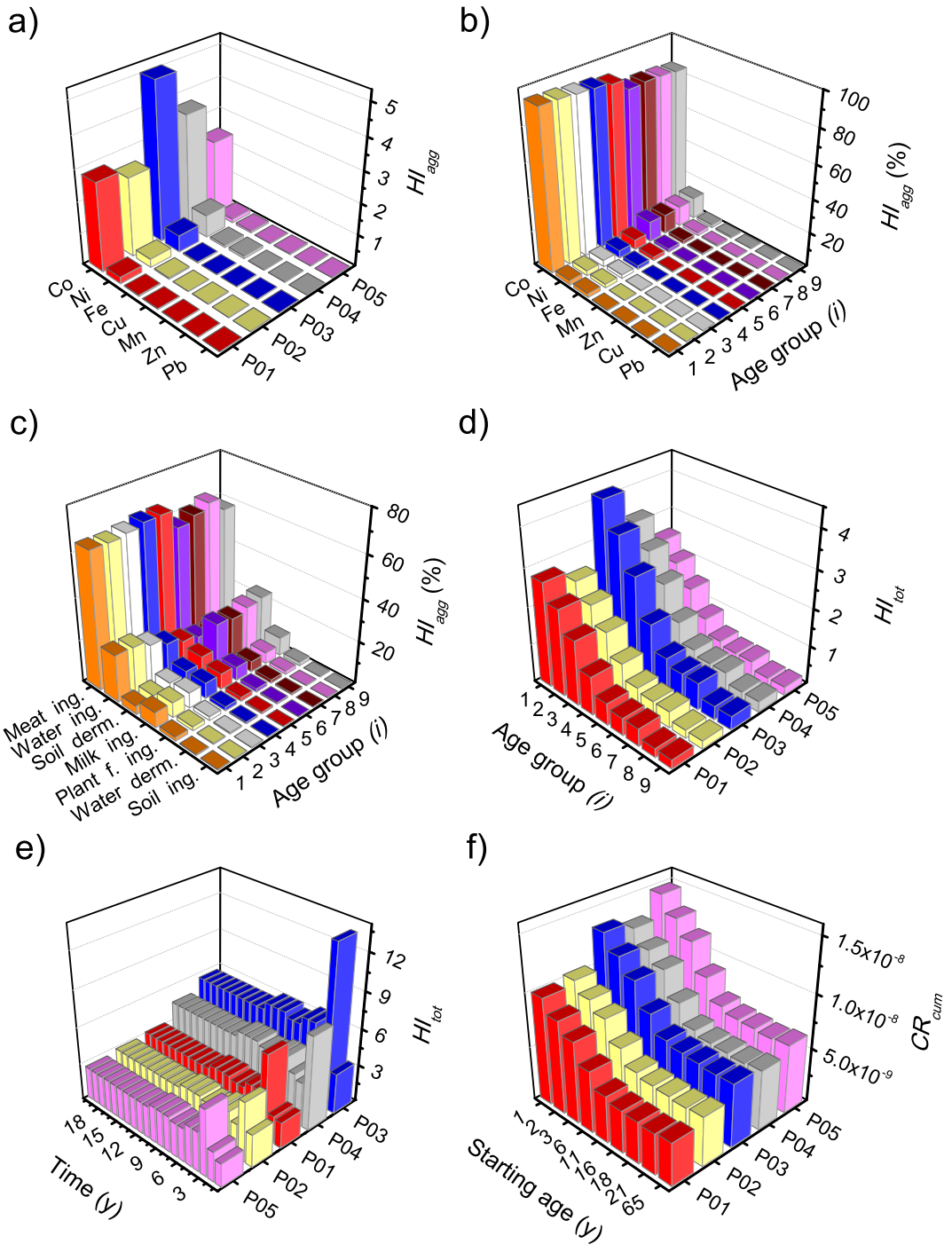

Fig. 4. Analysis of the human health risks in the nickel mining area of the municipality of Itagibá (Bahia, Brazil). a) HI_{agg} specified by each sampling point. b) Contribution (%) of each metal to total HI_{agg} for each age group. c) Contribution (%) of each exposure pathway to the total HI_{agg} for each age range. d) HI_{tot} for acute exposure for each age group specified by local. e) Spatiotemporal HI_{tot} analysis for chronic exposure (20 year) specified by local. f) Final carcinogenic risk after 20 years of exposition to Pb for different initial ages of exposure (*IA*) and locals. Age groups: 1 (*1 to 2 years*), 2 (*2 to 3 years*), 3 (*3 to 6 years*), 4 (*6 to 11 years*), 5 (*11 to 16 years*), 6 (*16 to 18 years*), 7 (*18 to 21 years*), 8 (*21 to 65 years*), and 9 (*>65 years*).

for the age range 21–65. The risk associated with the consumption of plant foods did not exceed 2.5%; therefore, it does not pose a threat.

The ingestion of contaminated water ranked fourth among the most dangerous exposure routes, with small variation between age groups (6–8%) (see Fig. 4c). The risk related to the dermal contact with contaminated water was below 1%. On the other hand, for soils, the opposite was observed: dermal contact posed a higher risk than the ingestion of soils. The results exhibited in Fig. 4c indicated that this exposure route plays a more decisive role for age ranges over 16 years, being responsible for up to 25.5% of the total risk in these age ranges, and below 12.2% for children (1 to <16 years). In the case of contaminated soil ingestion, the contribution to total risk was below 1.5% for all age ranges.

Fig. 4d shows the total hazard index (HI_{tot}) associated with the acute exposure events. This figure aimed to explore in more detail the variation of the hazard index for the nine age ranges considered in the code. As can be noticed, the average HI_{tot} values decreased with age (3.0 to 0.3). This result indicates that the non-carcinogenic risk associated with the exposure of PTE is higher for children, especially at early ages (1–11 years) than for adults, which could be related to the different

ingested concentration-body weight ratio, skin surface area available for contact and other physiological properties.

The information provided in Fig. 4d also emphasizes the pollution level of the regional water resources, as well as the risk they pose to human health. For children up to 11 years, the HI_{tot} ranged between 1.01 and 3.29, thus suggesting a moderate risk ($1 \leq HI_{tot} < 4$), except for the age range 1 to 2 years in P03, where HI_{tot} value was above 4 (high risk). For the other age ranges, the HI_{tot} values varied within the interval 0.1–1.0, which represents a low risk.

The spatio-temporal analysis of the chronic non-carcinogenic risk, *i.e.*, detailed year-by-year for each location of the studied region, is illustrated in Fig. 4e. Since a similar scenario was obtained for all age ranges, the HI_{tot} values for the age range 11 to 16 years, which is an intermediate age range, were displayed. As expected, the highest HI_{tot} values were found for the three first years, which correspond precisely to the sampling years. The P01 and P05 locations showed similar behavior, being the third year the one with the highest HI_{tot} value: 7.5 and 6.5, respectively, while for P02, the highest value (5.8) was observed in the second campaign. All these values are considered as high risk for human health ($HI_{tot} \geq 4$). From the fourth year, the estimated HI_{tot} values for these three locations (P01, P02, and P05) varied from 3.1 to 4.3, indicating a moderate to high risk.

The locations P03 and P04 were those with the highest risk to human health. The maximum value of HI_{tot} in P03 (15.0) corresponds to the second campaign, whereas for P04 was observed in the first campaign (8.5). Different from the other three locations, all the estimated HI_{tot} values from the fourth year are greater than 4; therefore, these locations are considered high risk for human health. These results show that, if proper care is not taken, the prolonged mining activity could cause severe damage to the ecosystems and the population of the region.

Fig. 4f shows the CR_{cum} values after 20 years of exposition to Pb for different initial ages of exposure (*IA*) in each location. The highest CR_{cum} values were observed in P05, which was the location with the highest average concentration of Pb in both soils and surface waters (see Tables S11 and S12, Supplementary Material). In general, carcinogenic risks for children were higher than adults; this is a result consistent with other studies (Doabi et al., 2018; Doležalová Weissmannová et al., 2019). All CR_{cum} values lay between $7.06 \cdot 10^{-9}$ and $4.36 \cdot 10^{-8}$, which are below 10^{-6}. For that reason, the carcinogenic risk for both children and adults can be considered negligible.

As can be seen in Table 2, the hazard index for mining areas generally exceeds 1.0. However, the *HI* values reported in this study greatly surpassed 1.0, indicating that the PTE concentrations found in the region may pose a severe non-carcinogenic risk to the surrounding population. On the other hand, the *CR* values remained within the safe range, while for the other mining areas are above $1 \cdot 10^{-4}$, which are unacceptable levels of carcinogenic risk. In general, both risks are greater for children, which reinforces that they are more susceptible to exposure to inorganic contaminants such as PTE due to their physiological and behavioral characteristics.

The HERisk code contains specific instructions to calculate the quantities uncertainties to characterize the human health risk evaluation adequately (Neris et al., 2019). Fig. S5 shows the variation of the relative uncertainty values for HI_{tot} and CR_{cum}. The σ_R values for HI_{tot} for all age groups reach up to 35%, while for CR_{cum}, the uncertainties were below 10%. These results are in agreement with the expected uncertainty values in the risk assessment, which are generally in the range of at least an order of magnitude or higher (Sassi et al., 2007).

To identify the parameters that most affected the uncertainties of the HI_{tot} results, the "budget of uncertainty" was performed (ISO, 2004; Neris et al., 2019). This analysis revealed that the *BAFs* uncertainties, which can reach up to ~90%, contributed most to the uncertainty of the final HI_{tot} value. This high contribution was not observed in the uncertainties associated with the CR_{cum} values, because Pb was the only metal considered in this calculation, and its maximum *BAFs* values reach ~35%.

5. Conclusion

This work aimed to describe the new HERisk code and to show its potential in assessing the ecological and human health risks associated with the presence of PTE in a mining area. Among the novelty of this new program, the following can be highlighted: a versatile input file (*.xlsm*) adaptable to the user's need, the inclusions of a new scenario (*in natura*) and two new subroutines ("***Radio_risk***" and "***Ecol_risk***"), intended for the evaluation of the radiological and ecological risks by computing more than 24 indices widely used in environmental studies. The HERisk also considers age-dependent exposure parameters and different types of exposure (acute, sub-chronic, and chronic), which allows us to assess human health risk more realistically.

The concentration of PTE (Co, Cu, Fe, Mn, Ni, Pb, and Zn) in soils and surface waters from the nickel mining area in the municipality of Itagibá (Bahia, Brazil) were studied. The obtained results show that metals are non-homogeneous distributed, suggesting the presence of local enrichment sources, mainly related to human activities. Although the mean concentration values of analyzed metals in soils did not exceed the permissible values established by Brazilian laws, the mean values of Co and Ni exceeded local background values. The contents of these elements in surface water reflect possible contamination of the regional water resources since the average concentrations for all metals are at least three times greater than the guideline values. The conducted statistical analyses revealed important metals interrelationships, indicating that mining and agricultural activities may be responsible for the contents of Co, Cu, Ni, Pb, and Zn in both soils and surface waters. The contents of Fe and Mn seem to be related to a geogenic source; however, a possible contribution from anthropogenic sources should not be overlooked.

The indices of pollution calculated confirmed anthropogenic pollution around the mining area, especially in the sampling points closest to sterile waste piles. In general, the soils showed a low degree of contamination for most of the metals, except for Co and Ni that exhibited moderate pollution. A different picture was observed for surface waters, where all indices indicated that water resources could be classified as extremely polluted. Likewise, 80% of the values of the *PERI* in surface waters were above 720, indicating a highly strong ecological risk.

The results of the HHRE revealed that: (1) Co is the chemical species that pose the highest risk in the entire region; (2) the ingestion of meat and contaminated water are the main routes for entering the PTE to human body; (3) *HI* values greater than four (high risk) were observed for at least one campaign in all locations and the values estimated during the whole exposure time (20 years) indicated that P03 and P04

Table 2
Maximum *HI* and *CR* values reported for other mining areas around the world.

Country	Main pollutants	*HI*		*CR* (10^{-6})		Reference
		Adults	Children	Adults	Children	
China	As, Cd, Ni	15.7	19.2	4390	2130	Li et al. (2014)
Czech Republic	V, Pb, Zn	2.19	2.07	136	1270	Doležalová Weissmannová et al. (2019)
Ghana	As, Pb, Cu	0.23	2.18	46.7	4360	Hadzi et al. (2019)
Brazil	Co, Ni, Fe	13.0	49.6	0.02	0.04	This study

should be considered high risk for human health; (4) the carcinogenic risk for both children and adults can be considered very low.

Finally, the HERisk code has proven to be a crucial tool for characterizing the risk associated with exposure to chemical pollutants and for estimating its variation during specific periods. Precisely, its application on the nickel mining area in Itagibá revealed the urgency of paying more attention to PTE contamination in this region. If proper care is not taken, the continuous mining activity may become a threat not only to the equilibrium of the ecosystem but also to the health of the local population, which makes use of the resources (soils and waters) for their sustenance.

CRediT authorship contribution statement

Jordan Brizi Neris: Conceptualization, Software, Writing – original draft, Formal analysis, Data curation, Resources. **Diango M. Montalván Olivares:** Conceptualization, Writing – original draft, Formal analysis. **Caroline Santos Santana:** Methodology, Investigation, Writing – original draft. **PraiseGod Chidozie Emenike:** Writing – review & editing, Visualization. **Fermin G. Velasco:** Resources, Writing – review & editing, Supervision. **Sergio Fred Ribeiro Andrade:** Methodology, Investigation. **Caio Marcio Paranhos:** Writing – review & editing.

Declaration of competing interest

The authors declare that they have no known competing financial interests or personal relationships that could have appeared to influence the work reported in this paper.

Acknowledgments

The authors are grateful to both the National Council for Scientific and Technological Development - Brazil (CNPq) and Coordination for the Improvement of Higher Education Personnel (CAPES) for providing doctoral scholarships. Likewise, we thank the Center for Research in Radiation Sciences and Technologies (CPqCTR) of the State University of Santa Cruz (UESC), for the logistical support provided for the collection and analysis of samples.

Appendix A. Supplementary data

Supplementary data to this article can be found online at https://doi.org/10.1016/j.scitotenv.2021.145044.

References

Adewumi, A.J., Laniyan, T.A., 2020. Ecological and human health risks associated with metals in water from Anka Artisanal Gold Mining Area, Nigeria. Hum. Ecol. Risk Assess. An Int. J. 0, 1–20. https://doi.org/10.1080/10807039.2019.1710694.

Alam, M., Hussain, Z., Khan, A., Khan, M.A., Rab, A., Asif, M., Shah, M.A., Muhammad, A., 2020. The effects of organic amendments on heavy metals bioavailability in mine impacted soil and associated human health risk. Sci. Hortic. (Amsterdam). 262, 109067. https://doi.org/10.1016/j.scienta.2019.109067.

Atlantic Nickel, B.R., 2020. Mina Santa Rita - Home [Online], Itagibá: Atlantic Nickel BR [WWW Document]. URL. http://atlanticnickel.com.

ATSDR, 2018. Minimal Risk Levels (MRLs), Agancy for Toxic Substances and Disease Registry.

Barnes, S.J., Osborne, G.A., Cook, D., Barnes, L., Maier, W.D., Godel, B., 2011. The Santa Rita nickel sulfide deposit in the Fazenda Mirabela Intrusion, Bahia, Brazil: geology, sulfide geochemistry, and genesis. Econ. Geol. 106, 1083–1110. https://doi.org/10.2113/econgeo.106.7.1083.

BGS, 2008. Nickel. British Geological Survey, Nottingham.

Biondi, C.M., Nascimento, C.W.A. do, Fabricio Neta, A. de B., Ribeiro, M.R., 2011. Teores de Fe, Mn, Zn, Cu, Ni E Co em solos de referência de Pernambuco. Rev. Bras. Ciênc. Solo 35, 1057–1066. https://doi.org/10.1590/S0100-06832011000300039.

CBPM, 2009. Project Catalog [WWW Document]. Bahia Miner. Res. Company. Geol. Mapp.. URL. http://www.cbpm.ba.gov.br (accessed 5.30.20).

CBPM, 2020. Atlantic nickel studies expand reserves in Itagibá and may extend mine life by 26 years [WWW document]. URL. Bahia Miner. Res. Cohttp://www.cbpm.ba.gov.br/.

CETESB, 2001. Contaminated Area Management Manual. Environmental Company of The State Of São Paulo, São Paulo.

CETESB-ANA, 2011. National Guide for Sample Collection and Preservation: Water, Sediment, Aquatic Communities and Liquid Effluents. Environ. Co.Natl. Water Agency, State São Paulo, p. 326.

CONAMA, 2005. Resolução. No. 357, de 17 de março de 2005. Dispõe sobre a classificação dos corpos de água e diretrizes ambientais para o seu enquadramento, bem como estabelece as condições e padrões de lançamento de efluentes, e dá outras providências. Conselho Nacional do Meio Ambiente, Diário Oficial [da] República Federativa do Brasil.

CONAMA, 2009. Resolução nº 420, de 28 de dezembro de 2009. Critérios e valores orientadores de qualidade do solo quanto à presença de substâncias químicas. Conselho Nacional do Meio Ambiente, Diário Oficial [da] República Federativa do Brasil.

Da Matta, G.N., 2016. Extração de níquel em rochas ultramáficas do déposito Santa Rita (Bahia). Federal University of Bahia, Bahia, Brazil.

Doabi, S.A., Karami, M., Afyuni, M., Yeganeh, M., 2018. Pollution and health risk assessment of heavy metals in agricultural soil, atmospheric dust and major food crops in Kermanshah province, Iran. Ecotoxicol. Environ. Saf. 163, 153–164. https://doi.org/10.1016/j.ecoenv.2018.07.057.

Doležalová Weissmannová, H., Mihočová, S., Chovanec, P., Pavlovský, J., 2019. Potential ecological risk and human health risk assessment of heavy metal pollution in industrial affected soils by coal mining and metallurgy in Ostrava, Czech Republic. Int. J. Environ. Res. Public Health 16, 4495. https://doi.org/10.3390/ijerph16224495.

Emenike, P.C., Tenebe, I.T., Neris, J.B., Omole, D.O., Afolayan, O., Okeke, C.U., Emenike, I.K., 2020. An integrated assessment of land-use change impact, seasonal variation of pollution indices and human health risk of selected toxic elements in sediments of River Atuwara, Nigeria. Environ. Pollut. 265, 114795. https://doi.org/10.1016/j.envpol.2020.114795.

Fairweather-Tait, S., Hurrell, R.F., 1996. Bioavailability of minerals and trace elements. Nutr. Res. Rev. 9, 295–324. https://doi.org/10.1079/NRR19960016.

Guo, X., Xie, X., Liu, Y., Wang, C., Yang, M., Huang, Y., 2020. Effects of digestate DOM on chemical behavior of soil heavy metals in an abandoned copper mining areas. J. Hazard. Mater. 393, 122436. https://doi.org/10.1016/j.jhazmat.2020.122436.

Gyamfi, E., Appiah-Adjei, E.K., Adjei, K.A., 2019. Potential heavy metal pollution of soil and water resources from artisanal mining in Kokoteasua, Ghana. Groundw. Sustain. Dev. 8, 450–456. https://doi.org/10.1016/j.gsd.2019.01.007.

Hadzi, G.Y., Ayoko, G.A., Essumang, D.K., Osae, S.K.D., 2019. Contamination impact and human health risk assessment of heavy metals in surface soils from selected major mining areas in Ghana. Environ. Geochem. Health 41, 2821–2843. https://doi.org/10.1007/s10653-019-00332-4.

Hakanson, L., 1980. An ecological risk index for aquatic pollution control. A sedimentological approach. Water Res. 14, 975–1001. https://doi.org/10.1016/0043-1354(80)90143-8.

Health Canada, 2005. Guidance Document for Country Foods Surveys for the Purpose of Human Health Risk Assessment (Canada).

Helsley, R.N., Zhou, C., 2017. Epigenetic impact of endocrine disrupting chemicals on lipid homeostasis and atherosclerosis: a pregnane X receptor-centric view. Environ. Epigenetics 3, 1–15. https://doi.org/10.1093/eep/dvx017.

Hu, X., Zhang, Y., Luo, J., Wang, T., Lian, H., Ding, Z., 2011. Bioaccessibility and health risk of arsenic, mercury and other metals in urban street dusts from a mega-city, Nanjing, China. Environ. Pollut. 159, 1215–1221. https://doi.org/10.1016/j.envpol.2011.01.037.

Hu, J., Wu, F., Wu, S., Cao, Z., Lin, X., Wong, M.H., 2013. Bioaccessibility, dietary exposure and human risk assessment of heavy metals from market vegetables in Hong Kong revealed with an in vitro gastrointestinal model. Chemosphere 91, 455–461. https://doi.org/10.1016/j.chemosphere.2012.11.066.

IBGE, 2019. 2019 Sense. Brazilian Institute of Geography and Statistics.

IRMA, 2018. IRMA Water Quality Criteria by End-Use Tables. Initiative for Responsible Mining Assurance, Washington.

ISO, 1995. Soil Quality - Extraction of Trace Metals Soluble in Aqua Regia. International Organization for Standardization.

ISO, 2004. Guide to the Expression of Uncertainty in Measurement (GUM) – Supplement 1: Numerical Methods for the Propagation of Distributions. International Organization for Standardization, Geneva.

Jensen, J., Mesman, M., Rutgers, M., Breemen, L.D., Sorokin, N., ter Laak, T., Bierkens, J., Loibner, A.P., Erlacher, E., Ehlers, G.A.C., Bogolte, B.T., Celis, R., Hartnik, T., 2006. Ecological risk assessment of contaminated land - Decision support for site specific investigations. Rijksinstituut voor Volksgezondheid en Milieu RIVM.

Leggett, R.W., 2008. The biokinetics of inorganic cobalt in the human body. Sci. Total Environ. 389, 259–269. https://doi.org/10.1016/j.scitotenv.2007.08.054.

Li, Z., Ma, Z., Kuijp, T.J. van der, Yuan, Z., Huang, L., 2014. A review of soil heavy metal pollution from mines in China: pollution and health risk assessment. Sci. Total Environ. 468–469, 843–853. https://doi.org/10.1016/j.scitotenv.2013.08.090.

Marrugo-Negrete, J., Pinedo-Hernández, J., Díez, S., 2017. Assessment of heavy metal pollution, spatial distribution and origin in agricultural soils along the Sinú River Basin, Colombia. Environ. Res. 154, 380–388. https://doi.org/10.1016/j.envres.2017.01.021.

Mindat.org, 2020. Aplowite: Mineral Information and Data [Online] [WWW Document]. Hudson Inst. Mineral URL. https://www.mindat.org/min-282.html. (Accessed 6 May 2020).

Monteiro, N.B.R., da Silva, E.A., Moita Neto, J.M., 2019. Sustainable development goals in mining. J. Clean. Prod. 228, 509–520. https://doi.org/10.1016/j.jclepro.2019.04.332.

Neris, J.B., Olivares, D.M.M., Velasco, F.G., Luzardo, F.H.M., Correia, L.O., González, L.N., 2019. HHRISK: a code for assessment of human health risk due to environmental chemical pollution. Ecotoxicol. Environ. Saf. 170, 538–547. https://doi.org/10.1016/j.ecoenv.2018.12.017.

Newell, C.J., McLeod, K.R., Gonzales, J.R., 1996. BIOSCREEN - Groundwater Contamination Natural Attenuation Model (Version 1.3).

Pagliarini, É.C., Oliveira, V.B.D.M., Espindola, E.L.G., 2019. Ecological Risk assEssmEnt (ERa) application foR thE Evaluation of impacts on natuRal aquatic EcosystEms. Ambient. Soc. 22. https://doi.org/10.1590/1809-4422asoc0292r2vu19l1ao.

Pokorny, B., von Lübke, C., Dayamba, S.D., Dickow, H., 2019. All the gold for nothing? Impacts of mining on rural livelihoods in Northern Burkina Faso. World Dev. 119, 23–39. https://doi.org/10.1016/j.worlddev.2019.03.003.

Rafai, H.S., Newell, C.J., Gonzales, J.R., Dendrou, S., Dendrou, B., Kennedy, L., Wilson, J.T., 1998. BIOPLUME III Natural Attenuation Decision Support System.

Railsback, L.B., 2003. An earth scientist's periodic table of the elements and their ions. Geology 31, 737. https://doi.org/10.1130/G19542.1.

RIMA, 2006. Santa Rita Project - Nickel Ore Mining and Processing. Process CRA n. 2006-000986/TEC/LL-0013, Process DNPM n. 871.369/1989. Environmental Impact Report (Itajibá-Ba).

RIMA, 2011. Usina Termelétrica Barra do Rocha I. Environmental Impact Report.

Rudnick, R.L., Gao, S., 2014. Composition of the continental crust. Treatise on Geochemistry. Elsevier, pp. 1–51 https://doi.org/10.1016/B978-0-08-095975-7.00301-6.

Sassi, G., Vernai, A.M., Ruggeri, B., 2007. Quantitative estimation of uncertainty in human risk analysis. J. Hazard. Mater. 145, 296–304. https://doi.org/10.1016/j.jhazmat.2006.11.020.

da Silva, Yuri Jacques Agra Bezerra, do Nascimento, C.W.A., Cantalice, J.R.B., da Silva, Ygor Jacques Agra Bezerra, Cruz, C.M.C.A., 2015. Watershed-scale assessment of background concentrations and guidance values for heavy metals in soils from a semiarid and coastal zone of Brazil. Environ. Monit. Assess. 187, 558. https://doi.org/10.1007/s10661-015-4782-1.

Son, J., Kim, J.-G., Hyun, S., Cho, K., 2019. Screening level ecological risk assessment of abandoned metal mines using chemical and ecotoxicological lines of evidence. Environ. Pollut. 249, 1081–1090. https://doi.org/10.1016/j.envpol.2019.03.019.

Spence, L.R., Walden, T., 2001. RISC - users manual. Comput. Programs Biomed. 18, 99–108.

Stewart, R.N., Purucker, S.T., 2006. SADA: a freeware decision support tool integrating GIS, sample design, spatial modeling, and risk assessment. Int. Congr. Environ. Model. Softw. 427.

U.S. EPA, 1989. Risk Assessment Guidance for Superfund. Vol I: Human Health Evaluation Manual (Part A). U.S. Environmental Protection Agency.

U.S. EPA, 1994a. Method 3051: Microwave Assisted Digestion of Sediments and Sludges, Soils and Oils. United States Environmental Protection Agency.

U.S. EPA, 1994b. Method 200.8: Determination of Trace Elements in Waters and Wastes by Inductively Coupled Plasma – Mass Spectrofotometry. Revision 5,4. EMMC Version. United States Environmental Protection Agency.

U.S. EPA, 2004. Risk Assessment Guidance for Superfund Volume I: Human Health Evaluation Manual (Part E, Supplemental Guidance for Dermal Risk Assessment). U.S. Environmental Protection Agency.

U.S. EPA, 2005. Guidelines for Carcinogen Risk Assessment. U.S. Environmental Protection Agency.

U.S. EPA, 2007. Guidance for Evaluating the Oral Bioavailability of Metals in Soils for Use in Human Health Risk Assessment. U.S. Environmental Protection Agency.

U.S. EPA, 2009. Risk Assessment Guidance for Superfund Volume I: Human Health Evaluation Manual (Part F, Supplemental Guidance for Inhalation Risk Assessment). U.S. Environ. Prot. Agency.

US EPA, 2011. Exposure Factors Handbook. U.S. Environmental Protection Agency, USA.

Xie, Y., Xu, Y., Yan, L., Yang, R., 2005. Recovery of nickel, copper and cobalt from low-grade Ni–Cu sulfide tailings. Hydrometallurgy 80, 54–58. https://doi.org/10.1016/j.hydromet.2005.07.005.